Enhanced transmission through gratings: Structural and geometrical effects

Agnès Maurel
Institut Langevin, CNRS, ESPCI ParisTech, 1 rue Jussieu, 75005 Paris, France

Simon Félix
LAUM, CNRS, Université du Maine, avenue Olivier Messiaen, 72085 Le Mans, France

Jean-François Mercier
Poems, CNRS, ENSTA ParisTech, INRIA, 828 boulevard des Maréchaux, 91762 Palaiseau, France
(Received 23 May 2013; revised manuscript received 20 August 2013; published 10 September 2013)

Homogenization theory is used to derive the effective properties of gratings with complex subwavelength structures. Going beyond the effect of the filling fraction, geometrical effects are analyzed using a two-step homogenization process. An explicit expression for the transmission spectrum is derived, able to predict the Fabry-Perot resonances and the Brewster angle realizing broadband extraordinary transmission. With the same filling fraction, one expects from this analytical expression that gratings with different geometries may display very different transmission properties. This sensitivity to the microstructure geometry is exemplified in the case of gratings made of hard material and made of dielectric material. The analytical results are shown to be within a few percentage points as compared to full-wave numerical simulations, paving the way for transmission properties tuned by structural and geometrical manipulations.

DOI: 10.1103/PhysRevB.88.115416 PACS number(s): 78.67.−n, 43.20.Bi

I. INTRODUCTION

Since the pioneering works of Ebbesen,[1] many studies have been conducted on the enhanced transmission through subwavelength metallic gratings[2] or sound-hard gratings[3] (for a review, see Ref. 4). This extraordinary transmission (EOT in the context of optics and EAT in the context of acoustics) was primary based on resonances of surface waves (plasmon) and Fabry-Perot resonances, phenomena inherently limited in terms of frequency. More recently, broadband enhanced transmission has been reported.[5–8] This new EOT occurs at an optimal "Brewster" angle corresponding to the impedance matching between the host medium and the metallic grating. Lately, similar enhanced transmission has been reported in the context of acoustic waves for gratings made of impenetrable (sound-hard) material.[9,10] Although some studies have revealed the influence of the grating geometry,[11,12] structural and geometrical effects are in general disregarded. More generally, the gratings are composed by metallic layers for which the controlling parameter is the filling fraction and the attempts to propose simple analytical results were limited to this case.[6–10]

In this paper, we consider gratings made of penetrable material, rigid material being a limiting case. We show that the transmission spectra are accurately described by an analytical expression derived after homogenization has been applied, Eq. (4). This expression reveals that the transmission spectra can be strongly affected by geometrical effects, beyond the effect of the filling fraction only. In Sec. II, the case of single layers is considered. A generalization of the Brewster angle realizing the optimal transmission is obtained and this result is confirmed by comparison with direct numerical calculations. For more complex grating structures, a two-step homogenization is applied, leading to expressions of the effective parameters that account for the structural and geometrical characteristics of the grating, Eq. (9). This is done in Sec. III. Examples of the geometrical effects on the EOT are presented in Sec. IV in the nonmagnetic case [no contrast in B in Eq. (1)] and in the sound-hard case. The obtained results are validated by comparison with direct numerical calculations. Technical calculations on the two-step homogenization are collected in the appendix.

II. EXTRAORDINARY TRANSMISSION BY A SINGLE-LAYER STRUCTURE

The wave propagation in a grating made of penetrable material can be understood by solving the wave equation in an inhomogeneous medium written in the generic context of acoustic waves

$$\nabla\cdot\left[\frac{1}{\rho(\mathbf{r})}\nabla p(\mathbf{r})\right]+\frac{\omega^2}{B(\mathbf{r})}p(\mathbf{r})=0. \tag{1}$$

Here, the mass density ρ and the bulk modulus B can vary with position $\mathbf{r}$, allowing contrasts between the host medium (ρ,B) and the grating material (ρ_0,B_0). Equation (1) can be used with little modification for electromagnetic waves as for shallow water waves.

To begin with, the scattering of a plane wave $p^{(0)}$ at oblique incidence to a grating with single layer structure (SLG) is considered (a time-dependence $e^{-i\omega t}$ is understood throughout this paper). The grating has thickness l, with layers of width bd periodically located with d spacing (Fig. 1). In the low-frequency regime, the grating structure can be homogenized using the homogenization theory of layered media,[13] as used to build metamaterials.[14] It results that the grating can be replaced by an homogenized slab. The slab, of length l, is made of an homogeneous anisotropic medium described by the wave equation

$$\nabla\cdot\left[\begin{pmatrix}1/\rho_{\|} & 0\\ 0 & 1/\rho_{\perp}\end{pmatrix}\nabla p\right]+\frac{\omega^2}{B_e}p=0, \tag{2}$$

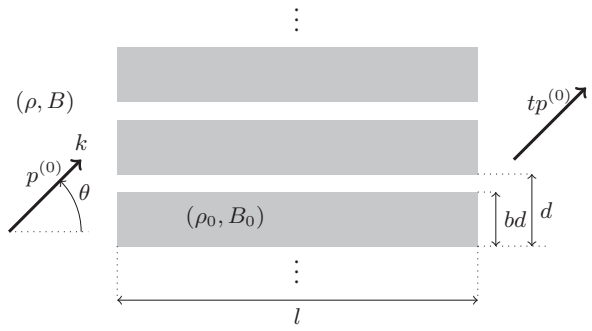

FIG. 1. The geometry of the single-layer grating (SLG).

with

$$\frac{1}{\rho_{||}} = \frac{b}{\rho_0} + \frac{(1-b)}{\rho}, \quad \rho_\perp = b\rho_0 + (1-b)\rho,$$
$$\frac{1}{B_e} = \frac{b}{B_0} + \frac{(1-b)}{B}. \tag{3}$$

The transmission coefficient t is

$$t = \frac{4ue^{ikl\cos\theta}}{(1+u)^2 e^{-ik_\parallel l} - (1-u)^2 e^{ik_\parallel l}}, \tag{4}$$

with

$$u \equiv \frac{k\cos\theta}{k_\parallel}\frac{\rho_{||}}{\rho} \tag{5}$$

being the ratio of the effective impedances and where $k_\parallel$ is the effective horizontal wavenumber, given by the dispersion relation [from Eq. (2)]:

$$k_\parallel^2/\rho_{||} + k^2\sin^2\theta/\rho_\perp = \omega^2/B_e. \tag{6}$$

The expression of t in Eq. (4) gives the standard Fabry-Perot resonances for $e^{ik_\parallel l} = \pm 1$ and the condition of perfect transmission (EOT) when the matched impedance condition is realized: $u = 1$. This homogenization has been already used in the Neumann limit[15] (note also that a non standard homogenization has been proposed in Ref. 8, where a more involved dispersion relation is used for $k_\parallel$). The Neumann limit corresponds to $\rho/\rho_0 \to 0$, $B/B_0 \to 0$, for which $k_\parallel \simeq k$ and $u \simeq \cos\theta/(1-b)$. Thus, the Fabry-Perot resonances are

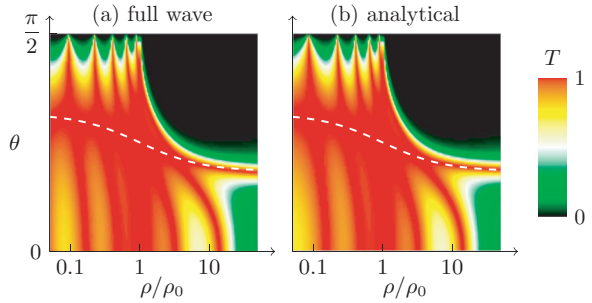

FIG. 2. (Color online) Transmission spectrum, $T = |t|^2$, as a function of the mass density contrast, ρ/ρ_0, and of the incidence angle, θ. The grating thickness is $l = 20d$. The layer width is $b = 0.7$ and the frequency is $kd = 0.5$. (a) Full-wave calculation, and (b) analytical result Eq. (4). The dashed line indicates the optimal angle, from Eq. (7).

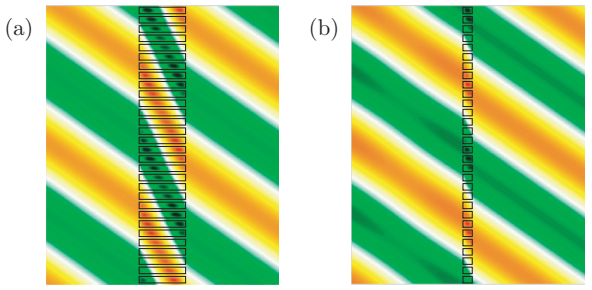

FIG. 3. (Color online) Spatial distribution of the wave field (real part) at frequency $kd = 1$ in a SLG grating with $b = 0.7$ and for $\rho/\rho_0 = 0.05$, at optimal angle, $\theta^{\text{opt}} \simeq 52.5^\circ$.

independent of the incidence angle and the matched impedance condition is obtained at the Brewster angle $\theta = \cos^{-1}(1-b)$, as reported in experiments performed using grating made of steel[15] or aluminum.[10]

Another limiting case corresponds to the case of water waves, or equivalently the case of p-polarized EM wave in a nonmagnetic dielectric grating. In this case, $B = B_0$ and only the contrast in ρ exists. Figure 2(b) shows the transmission spectrum, $T = |t|^2$, as a function of ρ/ρ_0 and as a function of the incidence angle θ, given by Eq. (4). A validation of this analytical result is done by computing a reference spectrum using full-wave numerical calculations.[16] Results are reported in Fig. 2(a): the difference between the two spectra is less than 3% in the whole range of incidence angles and contrasts. The Fabry-Perot resonances appear for certain combinations of $(\rho/\rho_0, \theta)$ that realize $k_\parallel l = n\pi$ and, contrary to the Neumann case, these resonances depend on the incidence angle since $k_\parallel$ does depend on θ. We have reported in Fig. 2 the optimal angle θ^{opt} realizing the condition of impedance matching, $u = 1$ in Eq. (5) using Eqs. (3) and (6),

$$\theta^{\text{opt}} = \cos^{-1}\sqrt{\frac{(1-b)\rho_0 + b\rho}{\rho_0 + \rho}}, \tag{7}$$

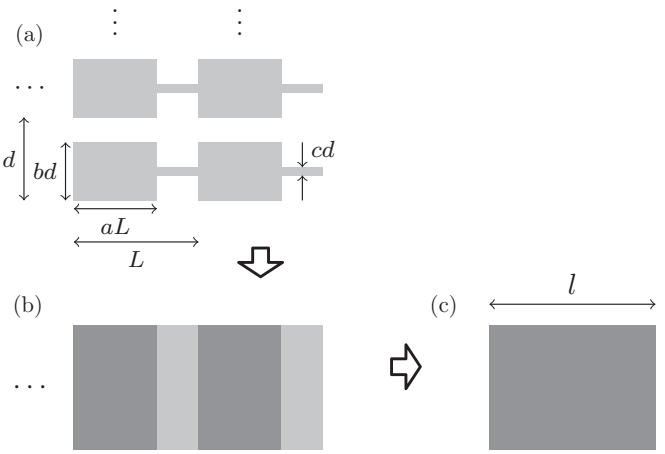

FIG. 4. Two-step homogenization. (a) Geometry of the double layer grating (DLG) including the case of rectangular inclusions (RIG) for $c = 0$. (b) The stack composed of two anisotropic layers of respective lengths aL and $(1-a)L$. (c) The resulting homogenized grating of length l.

from which the two limits for ρ/ρ_0 can be deduced:

$$\theta^{\text{opt}}(\rho/\rho_0 \to 0) = \cos^{-1}\sqrt{1-b},$$
$$\theta^{\text{opt}}(\rho/\rho_0 \to \infty) = \cos^{-1}\sqrt{b}, \tag{8}$$

and these two angles differ from the usual Brewster angle. The perfect transmission is independent of the length l of the grating, as illustrated in Fig. 3, for a small $\rho/\rho_0 = 0.05$ (gratings of lengths $l = 5d$ and $l = d$ are considered). In Fig. 3(a), for a small ρ/ρ_0, the wave propagating in the grating resembles the effective wave propagating with $k_\parallel \simeq k/(1-b)$, corresponding to a wavenumber inside the structure associated to an angle $\theta^{\text{eff}} = \cos^{-1}[1+b(1-b)]^{-1/2} < \theta^{\text{opt}}$.

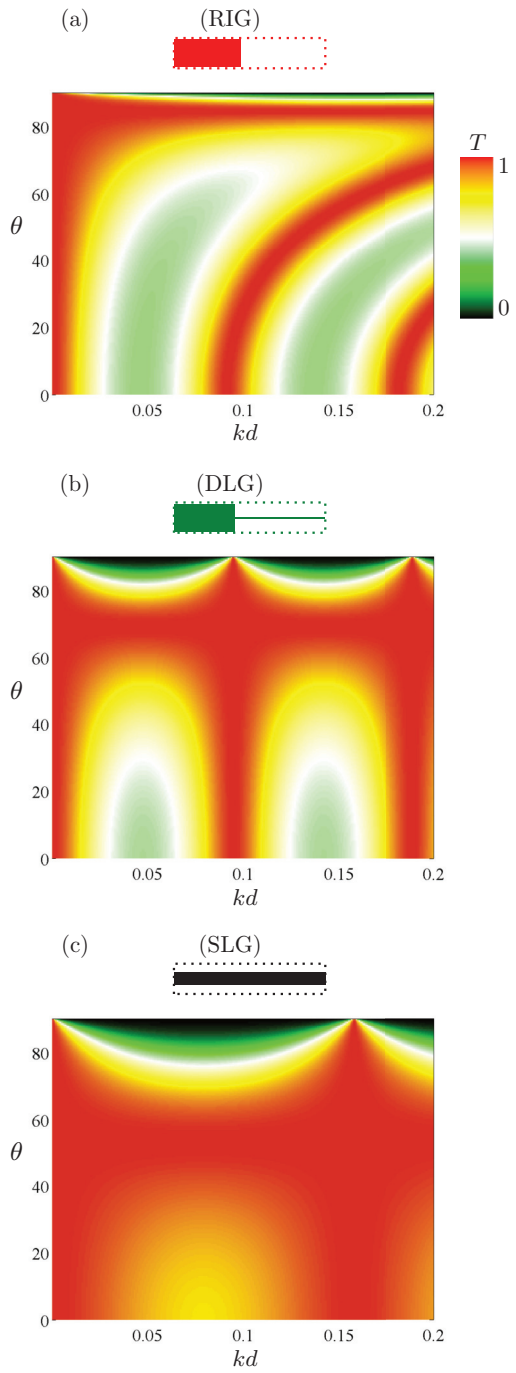

FIG. 5. (Color online) Transmission spectra of three gratings (rigid material), from Eq. (4), with Eqs. (5), (6), and (9). The gratings have the same filling fraction $\varphi = 0.4$ and different geometries. (a) (RIG) with $a = 0.44$ and $b = 0.9$ ($c = 0$); (b) (DLG) with $a = 0.4$, $b = 0.9$, and $c = 0.07$; and (d) (SLG) with $c = \varphi = 0.4$ ($a = 0$). Otherwise $L = 5d$ and $l = 20d$.

III. THE TWO-STEP HOMOGENIZATION

The robustness of the homogenization for small l values encourages the use of a further homogenization process for more complex grating structures, as sketched on Fig. 4. Our two-step homogenization is inspired from Ref. 17 for composite metamaterials. Our "composite" grating is made of a succession of layered structures with two different widths (bd and cd) alternatively stacked next to each other. Each layered structure is first homogenized as previously, resulting in a one-dimensional periodic succession of homogeneous anisotropic stacks of respective lengths aL and $(1-a)L$. This latter can be in turn homogenized to form a homogenized anisotropic effective medium, whose effective parameters are

$$\frac{\rho_\parallel}{\rho} = \frac{a}{b\rho/\rho_0 + 1 - b} + \frac{1-a}{c\rho/\rho_0 + 1 - c},$$
$$\frac{\rho}{\rho_\perp} = \frac{a}{b\rho_0/\rho + 1 - b} + \frac{1-a}{c\rho_0/\rho + 1 - c}, \tag{9}$$
$$\frac{B}{B_e} = [ab + (1-a)c]\frac{B}{B_0} + [1 - ab - (1-a)c],$$

and the inverse of the effective bulk modulus is simply the average of $1/B$ and $1/B_0$ with the filling fraction $\varphi \equiv [ab + (1-a)c]$ (see Appendix). In the following, we call double layer grating (DLG) the gratings formed by the succession of two layers of different widths b and c, and rectangular inclusion grating (RIG) refers to the particular case $c = 0$.

The expression of the transmission in Eq. (4), with Eqs. (5) and (6), is still valid with these new expressions of $\rho_\parallel$, $\rho_\perp$, and B_e, so that the Fabry-Perot resonances and the optimal

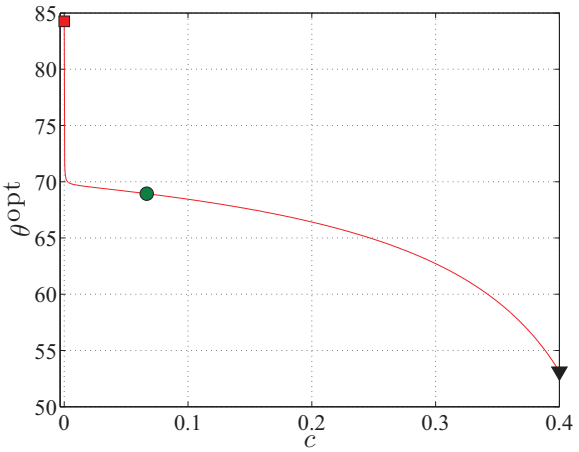

FIG. 6. (Color online) Influence of the parameter c on the optimal angle θ^{opt} realizing the matching impedance condition $u = 1$. The (DLG) varying c keep the same filling fraction $\varphi = 0.4$, with $b = 0.9$ and $a = (\varphi - c)/(b - c)$. The symbols refer to the gratings described in the legend of Fig. 5, (□): the (RI) on Fig. 5(a), (○) the (DLG) on Fig. 5(b), and (▽) the (SLG) on Fig. 5(c).

angle depend, now, in addition to the value of the contrasts and the filling fraction, on the geometry of the grating. For metallic grating, this geometry has been considered in Ref. 11 to enhance the transmission at normal incidence and, in this reference, this was done by decreasing the filling fraction. In fact, inspecting the Neumann limit ($\rho/\rho_0, B/B_0 \to 0$), one can see that the optimal angle for the SLG is always smaller than for any other structure with the same filling fraction.

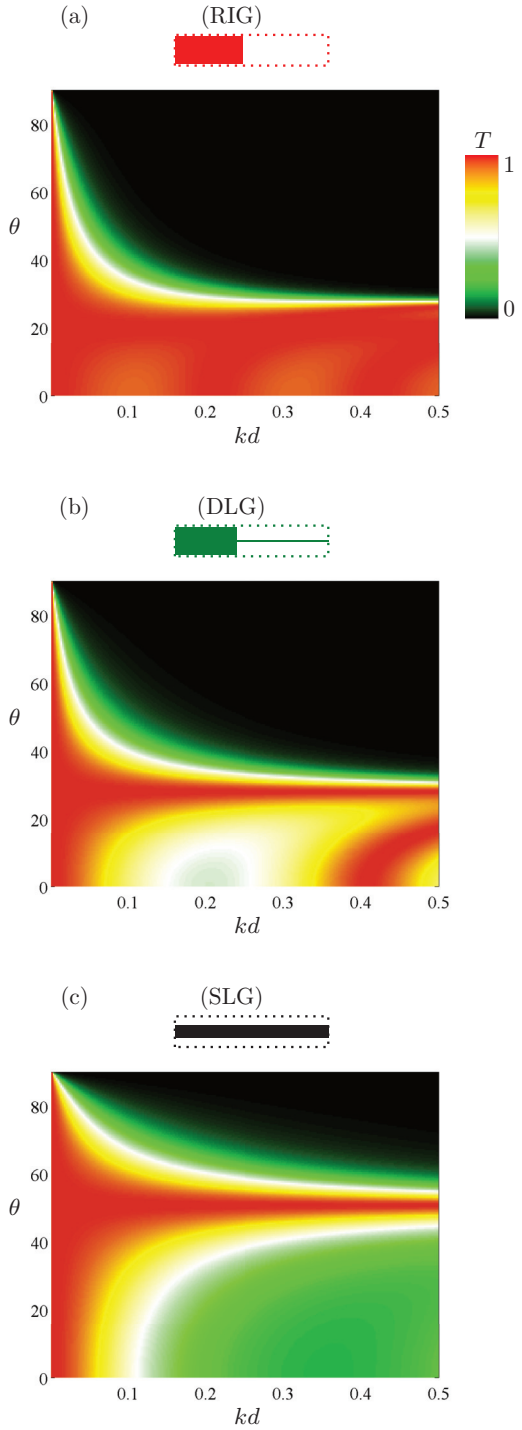

FIG. 7. (Color online) Same representation as described in the legend of Fig. 5 for nonmagnetic material ($B = B_0$) with $\rho/\rho_0 = 50$; the same grating geometries are presented.

IV. GEOMETRICAL EFFECTS ON THE EXTRAORDINARY TRANSMISSION

In the following, we exemplify the effect of the geometry by comparing the transmission spectra of different gratings with the same filling fraction.

First, we consider the limiting case of a rigid material. Figure 5 shows the transmission spectra of three gratings with different geometries and the same filling fraction $\varphi = 0.4$. The spectra have been calculated using Eq. (4), with Eqs. (5), (6), and (9) and the agreement with full-wave numerical computations (not reported) is very satisfactory (within few percents). The influence of the geometry on the spectra is visible, both on the Fabry-Perot resonances and on the impedance matching condition. This is inspected more quantitatively in Fig. 6, where the optimal angle θ^{opt} is plotted as a function of the parameter c. Varying c from 0 to φ, the grating geometry changes from the RIG geometry to the SLG, experiencing all the geometries of the DLG structures with the same filling fraction φ. From Fig. 6, one sees that the optimal angle θ^{opt} can be tuned continuously from about 70° to 52° by increasing c. The case $c = 0$ for which $\theta^{\text{opt}} \simeq 85°$ is a singular limit. Indeed, from Eq. (9), the effective mass density changes from $\rho/\rho_\perp = (1 - a)$ for $c = 0$ to $\rho/\rho_\perp = 0$ for $c \neq 0$ (with $\rho/\rho_0 \to 0$).

Next, we consider the case of a nonmagnetic dielectric material $B = B_0$ (a situation that applies without modification in the context of surface water waves propagating over an uneven bottom). Figure 7 shows the transmission spectra for a grating with $\rho/\rho_0 = 50$. A remarkable fact is the following: Although the RIG and the DLG gratings [in Figs. 7(a) and 7(b), respectively] have very similar geometries, the former grating acts as a low-angle pass filter while the latter behaves as a narrow-band angle filter (around the optimal angle) and, in both cases, for a wide range of frequencies. The influence of the grating geometry in terms of the parameter c is shown in Fig. 8: varying c produces a change in θ^{opt} from 20° to 50° for the same filling fraction $\varphi = 0.4$. A more subtle effect concerns the occurence of Fabry-Perot resonances. From Eqs. (9) and (6), the effective wavenumber $k_\parallel$ is smaller than k and it decreases when c increases (with constant φ and b). Thus, the

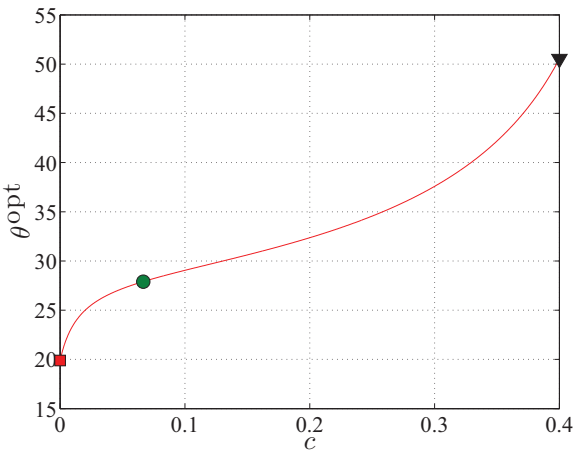

FIG. 8. (Color online) Same representation as described in the legend of Fig. 6 for the three gratings of Fig. 7.

Fabry-Perot resonances are sent to higher frequencies, resulting in angle filters working for larger frequency ranges.

V. CONCLUSIONS

In summary, homogenization has been shown to be a very efficient tool to analytically predict the transmission spectra of subwavelength gratings with complex geometry. The validity of our prediction has been checked by comparison with full-wave numerical computations. Also, we extended the study to the case of penetrable gratings. This is of interest when considering electromagnetic waves propagating in dielectric material and when considering surface water wave over an uneven bottom. The obtained expression for the transmission spectra allows us to exhibit the geometrical effects, beyond the effect of the filling fraction usually considered. Obviously, the advantage of such analytical results is to be predictive: the description of gratings with variable contrasts and complex geometries involves more and more parameters and using direct numerical computations would be too fastidious to inspect their influences on the transmission.

Our works open a promising way for the design of gratings with transmission properties controlled by structural and geometrical manipulations. Potential applications include directive antenna and directive loudspeakers, antinoise walls, lenses design, and water-wave focusing.

ACKNOWLEDGMENT

The authors acknowledge the financial support of the Agence Nationale de la Recherche through the Grant ANR ProCoMedia, Project No. ANR-10-INTB-0914.

APPENDIX: THE TWO-STEP HOMOGENIZATION

We report the main steps leading to Eq. (9). To do that, we first use classical homogenization of layered medium (1) with horizontal layers (Fig. 1). We get, for layers of filling fraction b

$$\nabla \cdot \left[\begin{pmatrix} 1/\rho_{||}^{(b)} & 0 \\ 0 & 1/\rho_{\perp}^{(b)} \end{pmatrix} \nabla p \right] + \frac{\omega^2}{B_e^{(b)}} p = 0, \tag{A1}$$

and we use, for ρ and B depending on the vertical direction (say y) $1/\rho_{||}^{(b)} = \langle 1/\rho(y) \rangle$, $\rho_{\perp}^{(b)} = \langle \rho(y) \rangle$ and $1/B_e^{(b)} = \langle 1/B_e(y) \rangle$, where $\langle f(y) \rangle \equiv (1/d) \int_0^d dy\ f(y)$ denotes the spatial average.

$$\begin{aligned} &\frac{1}{\rho_{||}^{(b)}} = \frac{b}{\rho_0} + \frac{(1-b)}{\rho}, \quad \rho_{\perp}^{(b)} = b\rho_0 + (1-b)\rho, \\ &\frac{1}{B_e^{(b)}} = \frac{b}{B_0} + \frac{(1-b)}{B}. \end{aligned} \tag{A2}$$

The same result applies for a medium (2) made of horizontal layers of filling fractions c and the resulting effective parameters are $\rho_{||}^{(c)}$, $\rho_{\perp}^{(c)}$ and $B_e^{(c)}$. The DLG structure consists in a succession of vertical layers of medium (1) and medium (2), as shown on Fig. 4(b). This DLG structure can be homogenized, considering the filling fraction a for the medium (1) [and $(1-a)$ for the medium (b)]. The structure has now effective parameters varying along the horizontal direction (say x), so that the homogenization of the layered structure is such that $\rho_{||} = \langle \rho_{||}(x) \rangle$, $1/\rho_{\perp} = \langle 1/\rho_{\perp}(x) \rangle$, and $1/B_e = \langle 1/B_e(x) \rangle$.

We get a resulting homogenized anisotropic structure [as in Eq. (3)], with

$$\begin{aligned} &\rho_{||} = a\rho_{||}^{(b)} + (1-a)\rho_{||}^{(c)}, \quad \frac{1}{\rho_{\perp}} = \frac{a}{\rho_{\perp}^{(b)}} + \frac{(1-a)}{\rho_{\perp}^{(c)}}, \\ &\frac{1}{B_e} = \frac{a}{B_e^{(b)}} + \frac{(1-a)}{B_e^{(c)}}, \end{aligned} \tag{A3}$$

leading to the expressions in Eq. (9).

[1] T. W. Ebbesen, H. J. Lezec, H. F. Ghaemi, T. Thio, and P. A. Wolff, Nature (London) **391**, 667 (1998).

[2] U. Schröter and D. Heitmann, Phys. Rev. B **58**, 15419 (1998); J. A. Porto, F. J. García-Vidal, and J. B. Pendry, Phys. Rev. Lett. **83**, 2845 (1999).

[3] M-H. Lu, X.-K. Liu, L. Feng, J. Li, C.-P. Huang, Y.-F. Chen, Y.-Y. Zhu, S.-N. Zhu, and N.-B. Ming, Phys. Rev. Lett. **99**, 174301 (2007).

[4] F. J. García-Vidal, L. Martín-Moreno, T. W. Ebbesen, and L. Kuipers, Rev. Mod. Phys. **82**, 729 (2010).

[5] X-R. Huang, R-W. Peng, and R-H. Fan, Phys. Rev. Lett. **105**, 243901 (2010).

[6] A. Alù, G. D'Aguanno, N. Mattiucci, and M. J. Bloemer, Phys. Rev. Lett. **106**, 123902 (2011).

[7] N. Aközbek, N. Mattiucci, D. de Ceglia, R. Trimm, A. Alù, G. D'Aguanno, M. A. Vincenti, M. Scalora, and M. J. Bloemer, Phys. Rev. B **85**, 205430 (2012).

[8] C. Argyropoulos, G. D'Aguanno, N. Mattiucci, N. Akoztek, M. J. Bloemer, and A. Alù, Phys. Rev. B **85**, 024304 (2012).

[9] C. Qiu, R. Hao, F. Li, S. Xu, and Z. Liu, Appl. Phys. Lett. **100**, 191908 (2012).

[10] G. D'Aguanno, K. Q. Le, R. Trimm, A. Alù, N. Mattiucci, A. D. Mathias, N. Aközbek, and M. J. Bloemer, Sci. Rep. **2**, 340 (2012).

[11] G. Subramania, S. Foteinopoulou, and I. Brener, Phys. Rev. Lett. **107**, 163902 (2011).

[12] H. Shen and B. Maes, Appl. Phys. Lett. **100**, 241104 (2012).

[13] A. Bensoussan, J. L. Lions, and G. Papanicolaou, *Asymptotic Analysis for Periodic Structures* (North-Holland, Amsterdam, 1978).

[14] J. Li, L. Fok, X. Yin, G. Bartal, and X. Zhang, Nat. Mater. **8**, 931 (2009).

[15] D.-X. Qi, R.-H. Fan, R.-W. Peng, X.-R. Huang, M.-H. Lu, X. Ni, Q. Hu, and M. Wang, Appl. Phys. Lett. **101**, 061912 (2012).

[16] Full-wave calculations have been done using a coupled wave method, as described in, e.g., E. Popov, and M. Neviére, J. Opt. Soc. Am. **17**, 1773 (2006).

[17] A. I. Cabuz, D. Felbacq, and D. Cassagne, Phys. Rev. Lett. **98**, 037403 (2007).